International Journal of Thermophysics, Vol. 9, No. 2, 1988

Internal Stress and Solid Solubility Effects on the Thermal Expansivity of Al–Si Eutectic Alloys[1]

T. A. Hahn[2] and R. W. Armstrong[3]

Thermal expansion measurements are reported for a number of as-cast Al–Si eutectic alloys including a Sr-modified alloy which gives nearly spherical Si particles. The measurements were obtained by heating and cooling over repeated temperature cycles between room temperature and 500°C. In general, lower expansivity values were measured on the cooling cycle as compared with the heating cycle, resulting in a net positive permanent deformation at room temperature. Analytical solutions are described for the thermal expansivity of a concentric-spheres model for a Si particle contained within an Al matrix. The effect of plastic flow in the Al is included. Overall, the predictions show reasonable agreement with the measured expansivities. The observed differences between heating and cooling are of the same order as that which is predicted. At high temperatures, the measured increase in expansivities is smaller than calculated. The latter effect is explained by the decrease in expansivity which results from an increasing solid solubility of silicon in aluminum with increasing temperature.

KEY WORDS: Al–Si eutectic alloys; concentric-spheres model; expansivities; solid solubility; thermal cycling; thermal expansion; thermal stresses.

1. INTRODUCTION

The thermal expansion properties of pure aluminum and its commercial alloys are well established. For example, the compilation of thermal expansion data by the Thermophysical Properties Research Center (TPRC) [1]

[1] Paper presented at the Ninth International Thermal Expansion Symposium, December 8–10, 1986, Pittsburgh, Pennsylvania, U.S.A.

[2] Composite Materials Branch, Naval Research Laboratory, Washington, D.C. 20375-5000, U.S.A.

[3] Department of Mechanical Engineering, University of Maryland, College Park, Maryland 20742, U.S.A.

0195-928X/88/0300-0179$06.00/0

contains more than 70 references for aluminum alone and, in addition, contains expansion data for more than 40 aluminum alloys.

Pioneering measurements of the thermal expansion of aluminum by Fizeau [2] were described over the relatively narrow temperature range $0°C \leqslant T \leqslant 90°C$ by the relation $L = L_0(1 + aT + bT^2)$, with $a = 22.21 \times 10^{-6}\ °C^{-1}$ and $b = 0.0114 \times 10^{-6}\ °C^{-2}$. The Fizeau measurements give the thermal expansivity $\alpha = a + 2bT = 22.67 \times 10^{-6}\ °C^{-1}$ at 20°C and $(d\alpha/dT) = 2b = 0.0228 \times 10^{-6}\ °C^{-2}$, thus showing a linear increase in α with an increase in the temperature. On a thermodynamic basis, Gruneisen has explained the temperature effect through relating the expansivity to the ratio of the specific heat capacity and the bulk elastic modulus [3].

For pure aluminum at very high temperatures, Simmons and Balluffi [4] measured the difference between the crystal lattice expansion and macroscopic length changes to obtain the concentration of atomic vacancies. Figure 1 shows the Simmons and Balluffi measurements in comparison with measurements obtained in the present study both for 1100 Al material and for an Al–0.12 Si eutectic alloy. Also shown in Fig. 1 are measurements for the repeated cycling of the Al–0.12 Si eutectic alloy leading to a permanent length change [5].

In fact, interesting results on the cyclic thermal expansion characteristics of Al–Si eutectic alloys were reported some time ago by Hidnert [6]. During repeated cycling between low and high temperatures, the

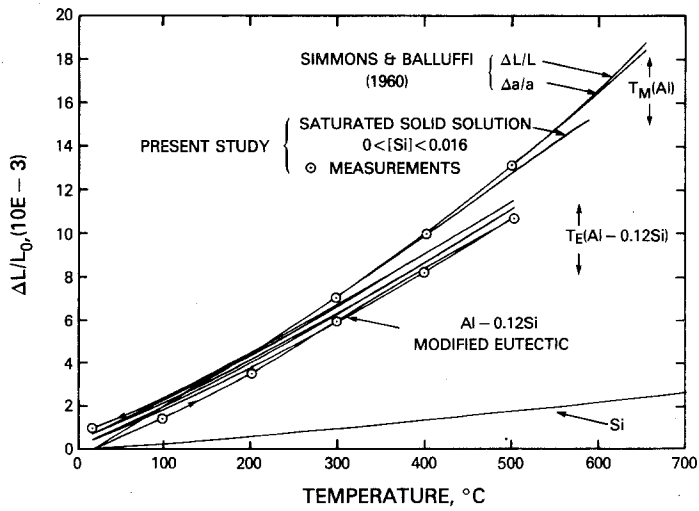

Fig. 1. Thermal expansion as a function of temperature for pure and 1100 Al, Si-saturated Al solid solution, Al–0.12 Si eutectic, and Si.

specimens were observed to grow in length. Presuming that the specimens were fully annealed, the most probable cause of the length changes must be plastic flow induced by the thermal stresses generated because of the mismatched expansivities of the aluminum and silicon phases. Liu and Gurland [7] have reported measurements by X-ray diffraction of significant internal stresses over the full composition range in the Al–Si alloy system.

On cooling the Al–Si eutectic alloy from high temperatures, the internal stresses were found by Liu and Gurland to be sufficient to cause plastic deformation of the aluminum matrix. Also, several models for evaluating the stress state within various Al–Si alloy compositions were described by Liu and Gurland, including a spherical or cylindrical inclusion contained within an infinite matrix. Hahn and Armstrong [8] used Fig. 2 to illustrate the relationship of internal pressure, P, to yield stress, σ_y, and plastic zone size, c, to inclusion radius, a, for various ratios of yield stress to Young's modulus for an internally compressed spherical model system proposed by Hill [9]. The hydrostatically pressurized spherical inclusion is assumed to cause plastic flow in the surrounding matrix material according to the Tresca shear stress-controlled theory of yielding.

In the present study, thermal expansion measurements are reported for repeated thermal cycling of three different Al–Si eutectic alloys. The gover-

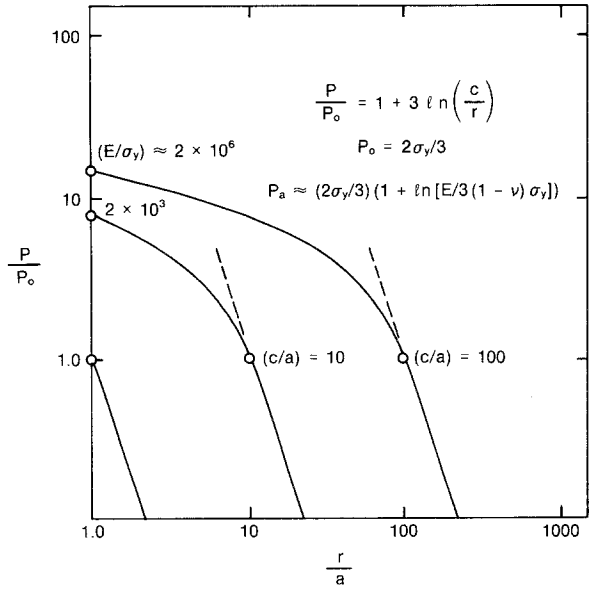

Fig. 2. Elastic–perfectly plastic analysis of radial stress for an inclusion in hydrostatic compression.

ning equations for a spherical particle included within a matrix shell are described in a related way for the several cases of a totally elastic system, an elastic–partially plastic shell with work hardening, and a fully plastic outer shell. The calculated value of α is shown to be reduced by a relatively small but increasing amount as the level of the internal stress increases. The greatest effect on α, which occurs for a fully plastic shell (with work hardening), is much smaller than has been measured. The plasticity effect appears to be more important in determining the different α measurements for the alloys than is their very different eutectic morphologies. Also, the effect of the increasing solid solubility of Si in Al with increasing temperatures is shown to have a significant effect on reducing α. The solid solubility effect is shown in Fig. 1 as determined from lattice parameter measurements associated with determining the Al–Si phase diagram [10, 11].

2. THERMAL EXPANSION OF Al–Si EUTECTIC ALLOYS

Accurate length measurements were obtained at 20, 100, and 100°C intervals extending to 500°C for three Al–0.12 Si eutectic alloys. Two of the alloys, an "as-cast" eutectic alloy and a Sr-modified alloy, were supplied by M. Kersker of the Aluminum Company of America (ALCOA). A laboratory as-cast alloy was supplied also by R. A. Meussner of the Naval Research Laboratory (NRL). The AlCOA modified alloy consisted of small essentially spherical Si particles with diameters less than 5 μm separated by an average distance of 8 μm. The as-cast ALCOA alloy contained much larger acicular Si particles. The NRL sample contained a greater range of Si particle sizes and shapes ranging through block, rod, and acicular morphologies, similar to the eutectic microstructures described by Liu and Gurland [7] for their internal stress measurements.

The current expansion measurements shown in Fig. 1 were obtained with a commercial fused quartz dilatometer (Anter Laboratories Model 1631) which is shown schematically in Fig. 3. The output of the instrument, which is under microcomputer control, is a digital signal for both the temperature and the length measurements. Sensitivities of 0.1°C in the temperature measurement and 1.0 μm in the length measurements were obtained by analog-to-digital conversion of the output of a platinum–platinum rhodium thermocouple, for the temperature measurement, and the output of a linear variable differential transformer (LVDT) for the length measurements. Using a sample length of 50 mm results in an expected uncertainty in the expansivity values of about 1%. The LVDT is situated above the furnace in a temperature-controlled chamber. A quartz rod, which rests on the sample, transmits the expansion of the sample to the

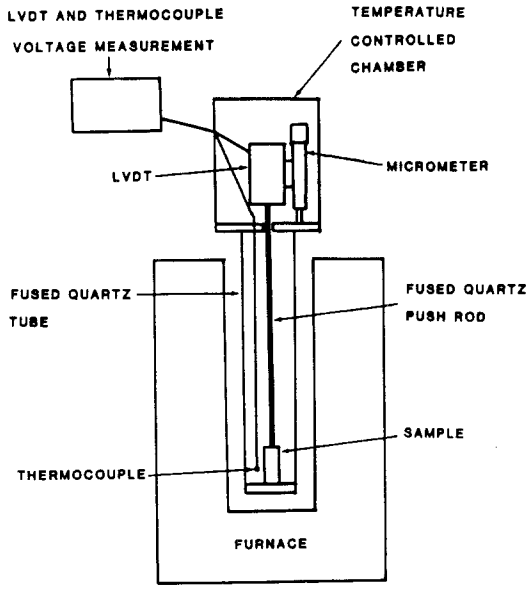

Fig. 3. Schematic representation of the push-rod dilatometer.

LVDT. The sample is supported within the furnace on a quartz flat that has been fused to the end of a quartz tube that is concentric with the sample and quartz rod. The temperature measurement thermocouple is situated next to the sample inside the quartz tube. The LVDT measurement coil assembly is connected to a micrometer, so that the output can be adjusted to zero voltage as the beginning of a test. The micrometer was also used to check the linearity of LVDT output voltage with displacement of the coil. The accuracy of this dilatometer is improved through the use of calibration standards according to ASTM test method E228 [12] for thermal expansion measurements with a fused quartz dilatometer.

For this study, a pure platinum sample, 50 mm in length, was used to calibrate the dilatometer. The standard was run periodically throughout the study to ensure the constancy of the correction values used in the calculation of the thermal expansion of the materials. The analytical expression of Hahn and Kirby [13] was used to calculate the expansion of the platinum at the experimental equilibrium temperatures. Use of the standard effectively corrects for nonuniformity in the LVDT, temperature measurement, electronics, and expansion of the quartz tube. Changes in supply voltage to the electronic circuits caused changes in the calibration of the measurement system. The supply voltage was therefore adjusted

whenever any changes were observed in its value. For a 50-mm sample length, the correction factor increased from zero at 20°C to an equivalent of $+0.35 \times 10^{-3}$ at 500°C. With the expansivity of fused quartz equal to 0.5×10^{-6} °C^{-1}, the expansion correction for the fused quartz would be 0.24×10^{-3}, which is therefore a major portion of the correction factor at 500°C.

The expansion values shown in Fig. 1 for 1100 aluminum agree well with the measurements reported by Simmons and Balluffi. The measurements were found to be reproducible over three cycles between 20 and 500°C as indicated in the second column in Table I. More interestingly, the expansion measurements given in Table I for each eutectic alloy, as indicated in Fig. 1 for the ALCOA modified alloy, exhibit a permanent change in length on the completion of each measurement cycle. The effect is cumulative for succeeding cycles, as shown in Fig. 1. An average increase in length of $(\Delta L/L) = 0.32 \times 10^{-3}$ was obtained for the ALCOA modified alloy after each cycle. The expansivity itself, which is the slope of the expansion curve, is reduced on the cooling portion of the cycle. Expansion values of the as-cast ALCOA and NRL samples are shown in Fig. 4 in comparison with the modified alloy results. The as-cast ALCOA sample exhibited an increase in length after each thermal cycle, with an average increase equal to 0.16×10^{-3} as shown in Table I. The average

Table I. Average Thermal Expansion $10^3 \Delta L/L$ of 1100 Al and Aluminum–Silicon Eutectic Alloys from 20°C to the Indicated Temperatures on Heating and Cooling[a]

			Eutectic alloy					
T (°C)	1100 Al		ALCOA modified		ALCOA normal		NRL	
20	0		0					
100	1.79	(0.02)	1.50	(0.05)	1.57	(0.02)	1.62	(0.02)
200	4.22	(0.06)	3.57	(0.06)	3.74	(0.02)	3.87	(0.02)
300	6.94	(0.05)	5.96	(0.08)	6.17	(0.03)	6.34	(0.04)
400	9.88	(0.01)	8.41	(0.06)	8.73	(0.03)	8.78	(0.05)
500	13.12	(0.06)	10.82	(0.05)	11.36	(0.03)	11.11	(0.04)
400	9.90	(0.04)	8.37	(0.08)	8.78	(0.03)	8.70	(0.04)
300	6.96	(0.03)	6.01	(0.08)	6.26	(0.03)	6.22	(0.04)
200	4.21	(0.01)	3.73	(0.05)	3.89	(0.02)	3.74	(0.05)
100	1.77	(0.02)	1.73	(0.09)	1.72	(0.02)	1.48	(0.05)
20	−0.01	(0.01)	0.32	(0.08)	0.16	(0.04)	−0.17	(0.07)

[a] Standard deviations are given in parentheses.

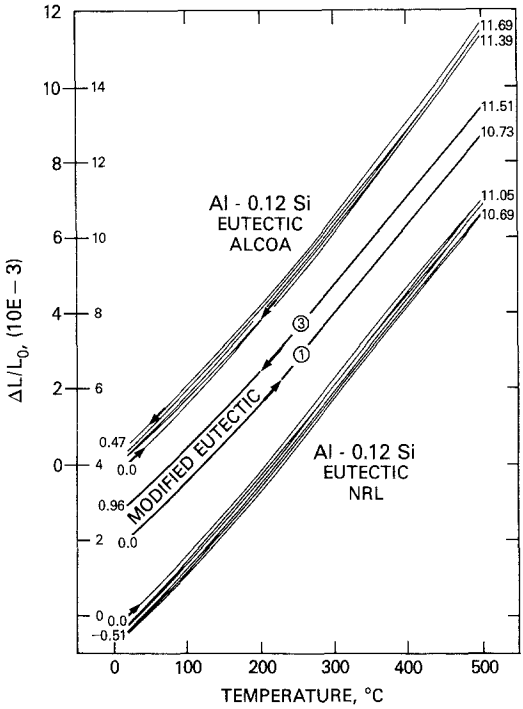

Fig. 4. Cyclic thermal expansion of the three Al–0.12 Si eutectic alloys.

total expansion of the as-cast ALCOA sample between 20 and 500°C is slightly greater than that of the modified alloy. In contrast to the two ALCOA samples, the NRL sample exhibited a decrease in length after thermal cycling, giving an average decrease of $(\Delta L/L) = -0.17 \times 10^{-3}$ as shown in Table I. The Sr-modified sample exhibited the smallest average expansion between 20 and 500°C.

The thermal expansivities, α, calculated from the expansion for the modified ALCOA, as-cast ALCOA, and NRL eutectic alloys are shown in Figs. 5–7. In Each case, the expansivity values for 1100 Al and for Si are also shown. The values for Si are from TPRC [1]. Theoretical α values computed on the basis of an elastic–plastic spherical model to be described are also shown in each case. In general, greater α values are obtained both experimentally and by model calculation on the heating portion of the thermal cycle. The vertical markers associated with each experimental point indicate the variation in the measurements.

The change in room-temperature length after one thermal cycle results naturally from the yield stress being lower at high temperatures and the

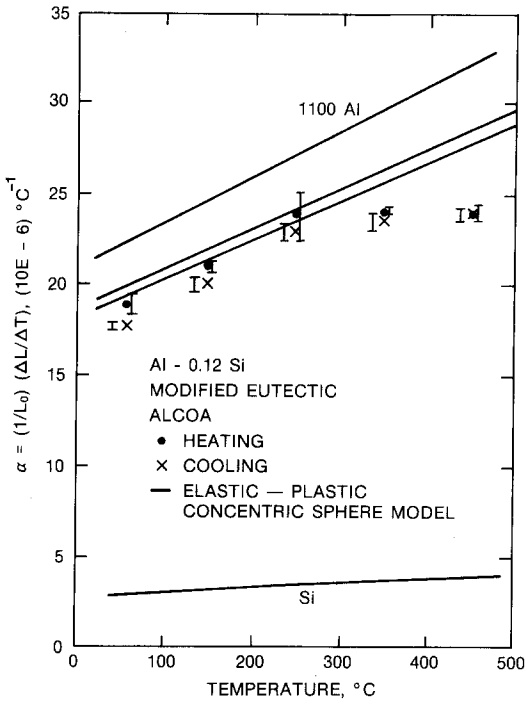

Fig. 5. Expansivity of Al–0.12 Si "modified" ALCOA eutectic alloy.

consequent reduction in α which occurs due to the matrix undergoing plastic deformation. An increase in length of the specimen should be expected to occur because of plastic flow. For example, beginning a heating cycle from 20°C, the residual stress in the Al (from the previous cooling cycle) is reduced elastically to zero and becomes tensile at high temperatures. According to calculations yielding occurs, approximately, above 200°C, with a concurrent small reduction in α. Upon reaching 500°C and reversing to the cooling part of the cycle, the tensile stress is now reduced to zero and becomes compressive again. The yield stress is lower at high temperatures so that yielding occurs after only a small reduction in temperature and the matrix undergoes plastic deformation for a greater portion of the cooling cycle. A lower α thus results from the smaller overall contraction which occurs on the cooling cycle. A net positive increase in length is achieved at room temperature. Depending on the increase in yield strength with decreases in temperature and especially on the work hardening, a specimen could exhibit a decrease in length with thermal cycling. This less typical behavior was obtained for the as-cast NRL material.

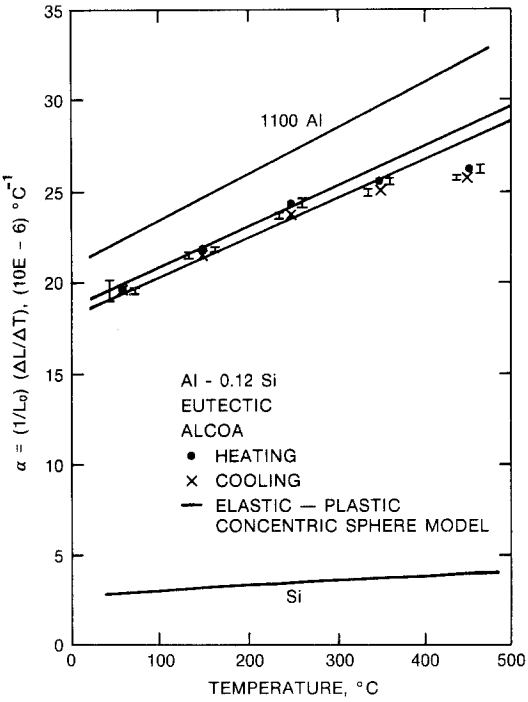

Fig. 6. Expansivity of Al–0.12 Si "as-cast" ALCOA eutectic alloy.

As was true for the total expansion measurements, greater α values are obtained for the two as-cast materials compared to the modified ALCOA alloy. At the higher temperatures, say, 250 to 500°C, the experimental rate of increase of α is substantially diminished for all three alloys. Both experimental observations are relatively surprising and have important consequences in the model explanation of the expansion properties for the Al–Si eutectic alloys.

3. MODEL EXPANSIVITY COMPARISONS

Figure 8 shows the theoretical dependence of α on the volume fraction of the included Si phase at 60°C in the Al–Si system subject to certain limiting conditions of constituent interactions and phase morphologies. The noninteracting rule of mixtures is seen to give the largest α values, which are progressively reduced by the occurrence of elastic stresses for the successive considerations of a spherical particle [14], an axial aligned cylindrical inclusion [15], a lamellar plate morphology [16], and the

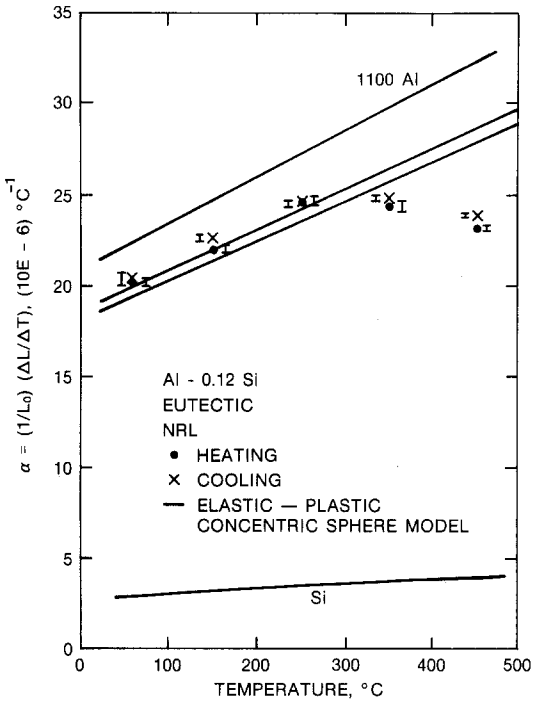

Fig. 7. Expansivity of Al–0.12 Si "as-cast" NRL eutectic alloy.

smallest α case obtained for a parallel circuit analogy [17]. The above models were derived considering mechanical interactions between the constituents. Schapery [18] has shown that the analyses are consistent with the minimum energy principle.

At the eutectic composition $V_1 = 0.12$ Si in Fig. 7 is shown the total range of α values obtained in the present study from the lowest cooling α result to the highest heating result. In contrast to the elastic model predictions, the experimental α values for (ALCOA modified) spherical particle systems are at the low end of the range which is shown and those α values for the rod-like as-cast microstructures are at the high end. However, in line with the morphology differences between the modified and the "as-cast" microstructures, the strength properties of the modified alloy are known to be substantially superior to those of the as-cast microstructures. The expectation, then, is that the α values for the modified eutectic alloy should be relatively low because of its internal stress and plastic deformation effects. For this reason, the effect of elastic stress and plastic flow on α has been examined in detail, in particular, for the case of a concentric spherical particle system.

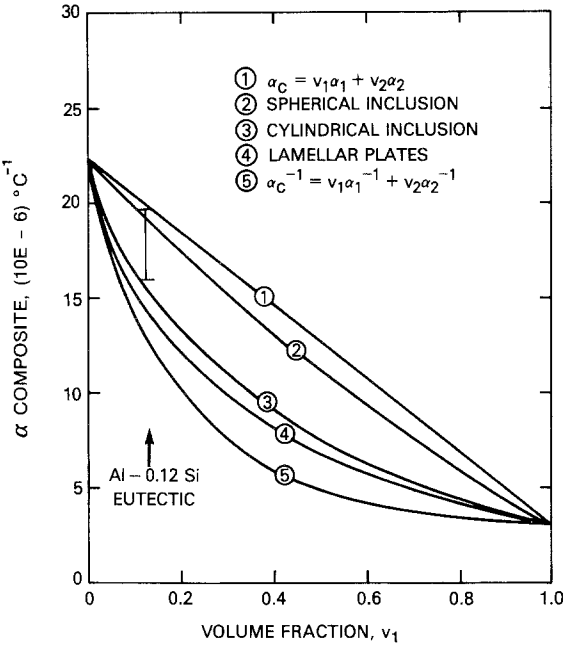

Fig. 8. Expansivities for various Al–Si model systems, with the range of measurements indicated for several Al–0.12 Si eutectic alloys.

The thermal expansivity, α_b, at the outer radius, b, of a totally elastic shell of material 2 containing an inner spherical particle of material 1, with radius a, also strained elastically, is obtained as [5, 14]

$$\alpha_b = \alpha_2 - (\alpha_2 - \alpha_1)\, V_1 \left(\left(\frac{1}{3K_2} + \frac{1}{4G_2} \right) \Big/ \left\{ \frac{1}{3} \left[\frac{1}{K_1} + \left(\frac{1}{K_2} - \frac{1}{K_1} \right) V_1 \right] + \frac{1}{4G_2} \right\} \right) \tag{1}$$

where K and G are the elastic bulk and shear moduli, respectively, for material 1 or 2. The value of $V_1 = (a/b)^3$. The value of K is connected with Young's modulus, E, and Poisson's ratio, v, by $K = E/3(1-2v)$. For two materials with identical elastic properties, Eq. (1) reverts to the rule of mixtures. With $K_2 = 68.9$ GPa and $G_2 = 26.4$ GPa for Al and $K_1 = 74.6$ GPa and $G_1 = 44.8$ GPa for Si, α_b is reduced below the rule of mixtures value as shown by curve 2 in Fig. 8.

When limited yielding occurs in material 2 according to the Tresca criterion and extends to a radius, c, such that $a \leqslant c \leqslant b$, then the α value for the elastically contained, partially plastic material is obtained as

$$\alpha_b = \alpha_2 - (\alpha_2 - \alpha_1)\, V_1 \times \left\{ \left[f\left(\frac{1}{3K_2} + \frac{1}{4G_2}\right)\right] \Big/ \left[\frac{1}{3} \left(\left\{ \frac{f-1}{K_1} + \frac{g}{3K_2} - \left(\frac{a}{c}\right)^3 \left[1 + \ln\left(\frac{c}{a}\right)^3 \right] \right. \right. \right.$$
$$\left. \left. \left. \times \left(\frac{1}{K_2} - \frac{1}{K_1}\right) \right\} + f\left(\frac{1}{K_2} - \frac{1}{K_1}\right) V_1 \right) + \left(\frac{g}{3}\right)\left(\frac{1}{4G_2}\right) \right] \right\} \tag{2}$$

where f and g are constants related to the linear work hardening of the plastic stress–strain curve of slope mE, in accordance with the equations $f = 1 + [2m/(1-m)](1-\nu_2)$ and $g = 3 + [2m/(1-m)](1+\nu_2)$. For $m = 0$, giving $f = 1$ and $g = 3$ and, also, $c = a$ at the very start of yielding, Eq. (2) reverts to Eq. (1). Otherwise, measurements of the extent of yielding given by c, as described by Hahn and Armstrong [8], may be thought to be used to determine the material yield stress, σ_y, according to the relationship

$$\sigma_y = \frac{3}{2} f(\alpha_2 - \alpha_1)\, \Delta T \left(\frac{a}{c}\right)^3 \Big/ \left[\frac{1}{3} \left(\left\{ \frac{f-1}{K_1} + \frac{g}{3K_2} - \left(\frac{a}{c}\right)^3 \left[1 + \ln\left(\frac{c}{a}\right)^3 \right] \right. \right.$$
$$\left. \left. \times \left(\frac{1}{K_2} - \frac{1}{K_1}\right) \right\} + f\left(\frac{1}{K_2} - \frac{1}{K_1}\right) V_1 \right) + \left(\frac{g}{3}\right)\left(\frac{1}{4G_2}\right) \right] \tag{3}$$

Equations (2) and (3) are in fact consistent with the analysis by Hill [9] in the limit $m = 0$ and $b = \infty$. The same result for Eq. (3) was obtained by Liu and Gurland [7]. For the opposite finite case of $c = b$, for which the matrix is totally plastic, then a new equation is obtained:

$$\alpha_b = \alpha_2 - (\alpha_2 - \alpha_1)\, V_1 \times \left(\left[3\left(\frac{f}{g}\right)\left(\frac{1}{2E_2}\right) \right] \Big/ \left\{ \frac{1}{g}\left(\frac{2m}{1-m}\right) \frac{1}{3} \left[\frac{1}{K_1} + \left(\frac{1}{K_2} - \frac{1}{K_1}\right) V_1 \right] + \frac{1}{2E_2} \right\} \right)$$
$$+ \left(\left[\frac{2}{3}\left(\frac{1}{g}\right)\left(\frac{1}{2E_2}\right)\left(\frac{\Delta\sigma_y}{\Delta T}\right)\left(\frac{1}{K_2} - \frac{1}{K_1}\right) V_1 \ln(1/V_1) \right] \Big/ \left\{ \frac{1}{g}\left(\frac{2m}{1-m}\right) \right.$$
$$\left. \times \frac{1}{3} \left[\frac{1}{K_1} + \left(\frac{1}{K_2} - \frac{1}{K_1}\right) V_1 \right] + \frac{1}{2E_2} \right\} \Bigg) \tag{4}$$

where $\Delta\sigma_y$ is the change in yield stress accompanying the temperature change ΔT.

In Eq. (4), with $m = 0 = \Delta\sigma_y/\Delta T$, the rule of mixtures equation for α_b is obtained. For $m = 1.0$, the system is elastic so that the third term in Eq. (4) is omitted, and the remainder of the equation, with $G_2 = E_2/2(1+\nu_2)$, goes over to Eq. (1).

Table II. Material Parameters Used in the Analysis for Comparison of the Various Analytical Models of the Thermal Expansion Coefficients of Composites[a]

	1100 Al				Si		
T (°C)	α (10^{-6} °C^{-1})	E (GPa)	ν	σ_y (MPa)	α (10^{-6} °C^{-1})	E (GPa)	ν
20	21.3	70.3	0.33	20	2.6	112	0.25
100	23.3	67.2	0.33	18	3.1	112	0.25
200	25.8	63.2	0.33	13	3.5	112	0.25
300	28.3	59.0	0.33	9	3.7	112	0.25
400	30.9	54.6	0.33	4	3.8	112	0.25
500	33.6	50.3	0.33	1	4.0	112	0.25

[a] Values are considered to be numerically equal on heating and cooling and in tension or compression.

The foregoing Eqs. (1) through (4) have been applied to computing α_b using the material properties listed in Table II. The computed α_b for a temperature increase was obtained on an elastic basis from Eq. (1) with simultaneous evaluation of the elastic stresses until the Tresca yield criterion was met for their differences [5]. Thereafter, values of c were obtained for further increases in temperature by inverting Eq. (3). These values of c were then substituted into Eq. (2) to obtain a continuing increase in α_b with increases in temperature. When c reached b, Eq. (4) was employed. Since the change in yield stress with temperature for Al is small, the predicted values of α_b are bounded in Figs. 5–7 by the predictions of Eq. (1), on the low side, based on elastic interactions and, on the high side, the rule of mixtures values. Close agreement between the experimental measurements and the predicted values of α_b are shown at low temperatures for the two as-cast alloys. In fact, the computed average value of α_b for a cylindrical model [19] is nearly equal to that predicted for the spherical case. The ALCOA modified eutectic alloy gives the lowest experimental α values, presumably because of its higher yield stress, greater work hardening, and resultant residual strain. Nevertheless, a larger reduction in α is measured at the lowest temperatures than can be accounted for with the current model.

At temperatures greater than approximately 400°C for the ALCOA modified alloy and the NRL as-cast material, the experimental values of α fell considerably below the estimated lower limiting values. This led to the consideration that α was being further reduced at high temperatures by Si going into solution in the matrix α phase (see Fig. 1).

The change in lattice parameter of aluminum with Si content was measured by Axon and Hume-Rothery [10] in the range from 0.23 to 0.93 atomic% Si. The lattice parameter decreased from 4.04081 to 4.03960 kX when the concentration increased from 0.23 to 0.93 atomic%. The equilibrium concentration of Si in Al as a function of temperature is reported by Hansen [11] from measurements carried out by Dix and Heath. The atomic concentration varied from 0.16 atomic% at 350°C to 1.59 atomic% at 577°C.

Since the solute concentration of Si in Al is dependent on the heat of solution, let the concentration be expressed by

$$C = Ae^{-\Delta H/RT} \tag{5}$$

A plot of (ln C) versus ($1/T$) gives $\Delta H = 45.5\ \text{kJ} \cdot \text{mol}^{-1}$ and $A = 994$. The lattice parameter of Al as a function of Si concentration can be expressed as

$$a = a_0 + \frac{\Delta a}{\Delta C} C \tag{6}$$

Differentiation with respect to temperature and division by the lattice parameter gives the coefficient α as

$$\alpha = \frac{1}{a_0}\frac{da}{dT} = \frac{1}{a_0}\frac{da_0}{dT} + \frac{1}{a_0}\left(\frac{\Delta a}{\Delta C}\right) Ae^{-\Delta H/RT}\left(\frac{\Delta H}{RT^2}\right) \tag{7}$$

where $(1/a_0)(da_0/dT)$ is the intrinsic lattice expansivity and the second term is the contribution due to the change in solute concentration. Using a value of $(\Delta a/\Delta C) = -1.73 \times 10^{-3}\ \text{kX}/(a/o)$ calculated from the Axon and Hume-Rothery data and A and ΔH as calculated from the Dix and Heath data results in a solute contribution to α of approximately $-2.2 \times 10^{-6}\ °\text{C}^{-1}$ at 450°C. This seems to explain the differences between the calculated and the experimental results for α at high temperatures in Figs. 5–7.

4. SUMMARY

(i) Thermal cycling of Al–Si eutectic alloys demonstrates plastic flow and solid solubility effects on the thermal expansion and on the expansivity.

(ii) The effect of both elastic stresses and plastic flow is to reduce α both experimentally and theoretically.

(iii) The solid solubility of Si in Al qualitatively accounts for the reduction in α at high temperatures greater than the lower bound on α_b for a totally plastic matrix.

REFERENCES

1. Y. S. Touloukian, R. K. Kirby, R. E. Taylor, and P. D. Desai, *Thermal Expansion—Metallic Elements and Alloys* (Plenum Press, New York, 1975), pp. 2–12.
2. *Handbook of Chemistry and Physics*, C. D. Hodgeman, ed. (Chemical Rubber Publishing Company, Cleveland, Ohio, 35th ed., 1953–1954), p. 2065.
3. R. A. Swalin, *Thermodynamics of Solids*, 2nd ed. (John Wiley and Sons, New York, 1972), p. 63.
4. R. O. Simmons and R. W. Balluffi, *Phys. Rev.* **34**:52 (1960).
5. T. A. Hahn, *Thermal Expansion Behavior and Analysis for Al-Si Eutectic Alloys and the Composite Material Systems: Al-SiC and Al-W*, Ph.D. dissertation (University of Maryland, College Park, 1986).
6. P. Hidnert, *Sci. Papers NBS 497* **19**:697 (1923–1924).
7. C. T. Liu and J. Gurland, *Trans. ASM* **58**:66 (1965).
8. T. A. Hahn and R. W. Armstrong, in *Thermal Expansion 7*, D. C. Larsen, ed. (Plenum Press, New York, 1982), p. 195.
9. R. Hill, *The Mathematical Theory of Plasticity* (Oxford University Press, London, 1956), p. 97.
10. H. J. Axon and W. Hume-Rothery, *Proc. Roy. Soc.* **A193**:1 (1948).
11. M. Hansen, *Constitution of Binary Alloys*, 2nd ed. (McGraw–Hill, New York, 1985).
12. *Annual Book of ASTM Standards, E228 (71) Standard Test Method* (ASTM, Philadelphia, 1980), p. 1041.
13. T. A. Hahn and R. K. Kirby, in *Thermal Expansion 1971* (Third Symposium), M. G. Graham and H. E. Hagy, eds. (Am. Inst. Phys. Conf. Proc. 1972), p. 87.
14. E. H. Kerner, *Proc. Phys. Soc.* **69B**:808 (1956).
15. P. S. Turner, *J. Res. NBS* **37**:239 (1946).
16. F. Laszlo, *J. Iron Steel Inst.* **148**:137 (1943).
17. J. P. Thomas, *General Dynamics Report FGT2713* (General Dynamics Corp., Fort Worth, Tex., 1960), AD287-826.
18. R. A. Schapery, *J. Comp. Mater.* **2**:380 (1968).
19. K. Wakashima, M. Otsuka, and S. Umekawa, *J. Comp. Mater.* **8**:391 (1974).